Journal of Biomolecular NMR (2006) 35: 225–239
DOI 10.1007/s10858-006-9024-y

Article

Backbone dynamics of a biologically active human FGF-1 monomer, complexed to a hexasaccharide heparin-analogue, by ^{15}N NMR relaxation methods

Angeles Canales-Mayordomo[a], Rosa Fayos[a], Jesús Angulo[b], Rafael Ojeda[b], Manuel Martín-Pastor[c], Pedro M. Nieto[b], Manuel Martín-Lomas[b], Rosa Lozano[a], Guillermo Giménez-Gallego[a] & Jesús Jiménez-Barbero[a,*]

[a]*Departamento de Estructura y Función de Proteínas, Centro de Investigaciones Biológicas, CSIC, Ramiro de Maeztu, 9, 28006, Madrid, Spain;* [b]*Grupo de Carbohidratos, Instituto de Investigaciones Químicas, CSIC, Américo Vespucios s/n, Isla de la Cartuja, 41092, Sevilla, Spain;* [c]*Laboratorio de Estructura e Estructura de Biomoléculas José Carracido, Unidad de RM y Unidad de RMN de Biomoléculas Asociada al CSIC, Santiago de Compostela, Spain*

Received 12 December 2005; Accepted 26 April 2006

Key words: chemical shift perturbation, fibroblast growth factors, heparan sulfate oligosaccharides, protein–carbohydrate interactions, relaxation analysis

Abstract

The binding site and backbone dynamics of a bioactive complex formed by the acidic fibroblast growth factor (FGF-1) and a specifically designed heparin hexasaccharide has been investigated by HSQC and relaxation NMR methods. The comparison of the relaxation data for the free and bound states has allowed showing that the complex is monomeric, and still induces mutagenesis, and that the protein backbone presents reduced motion in different timescale in its bound state, except in certain points that are involved in the interaction with the fibroblast growth factor receptor (FGFR).

Introduction

The human–mouse fibroblast growth factors (FGF) family consists of 22 members that share a common homologous core (Itoh and Ornitz, 2004). FGF-1 and −2 properties have been often considered paradigmatic for the whole family. Proteins including FGF-like domains have been also detected in invertebrates (Itoh and Ornitz, 2004). Fibroblast growth factors show a weak but statistically significant homology with interleukin-1β (IL-1β), which, however, never was considered a member of the FGF family (Giménez-Gallego et al., 1985; Itoh and Ornitz, 2004). FGFs are involved in a wide variety of physiological processes besides the control of cell division (Giménez-Gallego and Cuevas, 1994; White et al., 2000). They are also involved in many developmental steps during the embryogenesis. (Nishimura et al., 2000; Powers et al., 2000). The three-dimensional structure of several vertebrate FGFs have been determined using X-ray diffraction and NMR spectroscopy. The structure is homologous to that first described for soybean trypsin inhibitor (McLachlan, 1979). The fold, known as β-trefoil

*To whom correspondence should be addressed. E-mail: jjbarbero@cib.csic.es

motif, consists of six β-strand pairs which define a β-barrel capped at its base by three of the pairs. Five of the pairs have a hairpin structure ($\beta2-\beta3$, $\beta4-\beta5$, $\beta6-\beta7$, $\beta8-\beta9$, $\beta10-\beta11$). $\beta1$ and $\beta12$ are separate strands, but sometimes are also designed as the sixth hairpin because of their topological equivalence to the other strand pairs (Figure 1). There is some controversy about whether β-strand 11 really adopts such a canonical secondary structure, and whether it is more flexible than the rest (Pineda-Lucena et al., 1994, 1996; Moy et al., 1995; Ogura et al., 1999; Arunkumar et al., 2002a; Chi et al., 2002). FGF signaling begins at the target cell with the recognition of these growth factors by specific transmembrane tyrosine kinase receptors (FGFRs; Faham et al., 1998).

FGFs bind strongly to sulfated glycosaminoglycans (GAGs) of the type of heparin and heparan sulfate (HS) (Conrad, 1998; Capila et al., 2002; Itoh and Ornitz, 2004), a feature absent in IL-1β. *In vitro* assays have shown that FGF-2-induced mitogenesis is highly dependent on cell-surface heparan sulfate GAGs, although it can be replaced by soluble heparin (Yayon et al., 1991; Rapraeger et al., 1991; Ornitz et al., 1992). On the other side, heparin, itself, is a near absolute requirement for FGF-1-driven mitogenesis, in addition to cell-surface HS-GAGs. In this last case, heparin can be replaced by some non-physiological compounds of relatively low molecular mass. (Pineda-Lucena et al., 1994, 1996). There is a certain controversy about the minimal HS-GAG size required for this set of processes (Faham et al., 1998, Wu et al., 2003).

There is convincing evidence that FGF-1 and FGF-2 oligomerize to a certain extent in the presence of HS-GAGs (Waksman and Herr, 1998; Venkataraman et al., 1999). This oligomerization has been proposed to constitute a key step in physiological FGF-induce mitogenesis (Ornitz, et al., 1992; Spivak-Kroizman et al., 1994). According to the X-ray structures of FGFs complexed with heparin, and the NMR studies of FGFs bound to heparin functional analogs, it has been concluded that the main heparin binding site is located at the C-terminus, and that it involves residues belonging to the loop connecting strands XI and XII, and to X and XI strands. HS-GAGs seem also essential for the appropriate assemblage of an effective signaling complex between FGF and their cell membrane kinase receptors (Harmer et al. 2004a, b). The three-dimensional structures determined by X-ray diffraction show striking discrepancies in the proposed topologies of the GAG-protein interactions in both the binary FGF/GAG and ternary FGF/GAG/FGFR complexes (Faham et al., 1996; DiGabriele et al., 1998; Pellegrini et al., 2000; Schlessinger et al., 2000; Stauber et al., 2000). Sometimes FGF molecules assemble in *cis* orientation with respect to the GAG chain and others in *trans*. Since some of the studies have been carried out with FGF-1 and others with FGF-2, it cannot be excluded that the differences arise from the specific protein used in each case. There is an ongoing discussion on this point, although recent data seem to point towards the symmetric (*cis*) two-end model (Mohammadi et al., 2005a, b).

Synthetic GAG-type oligosaccharides may allow avoiding some of the problems that the inherent heterogeneity of the natural GAG fragments constitutes for high resolution structural characterizations. We have recently pioneered the use of those oligosaccharides for the structural characterization of the dependence of

Figure 1. Two different views of the ribbon diagram of FGF-1, showing the constituting 12 β-strands. The right panel shows the β-trefoil fold, with the 3-fold symmetry axis running through the center of the protein.

FGF-1-induced mitogenesis on heparin. We have shown that in the case of the "*natural*" sulfate distribution at both sides of the helix, typical of the native heparins, an octasaccharide is the minimum size of the synthetic GAG that can fully substitute heparins in the *in vitro* mitogenic assays. These last results are in agreement with results obtained with native heparins (Pellegrini, 2001). However, we have also demonstrated that hexasaccharide **1** (Figure 2) can substitute natural heparins in FGF-1 mitogenesis assays, in spite that it does not induce any apparent dimerization of the growth factor (Angulo et al., 2004). Hexasaccharide **1** is a synthetic heparin-like GAG, in which all the sulfate groups are oriented towards only one side of the typical helical-like structure adopted by heparin oligosaccharides. Therefore, the special topology of **1** should disfavor the dimerization of FGF caused by natural GAGs, thus simplifying the NMR analysis.

It is nowadays clear that many molecular recognition processes involve induced fitting. Dynamic properties play, obviously, a central role in these cases. Amino acid residues involved in ligand binding are frequently dynamic hot spots (Clackson and Wells, 1995; Atwell et al., 1997; Feher and Cavanagh, 1999), but internal motions, with different timescales, may additionally permit recognition elements to screen the allowed conformational space in search for the most energetically favorable fitting. Studies of the ^{15}N relaxation of the amide protons are able to provide information of a protein's dynamics from the pico- to the mili-second range (Korzhnev et al., 2001). Therefore they may substantially contribute to describe some of the relevant intramolecular protein's motions for a ligand recognition process, at very high resolution. Here the amide backbone dynamics of the monomeric FGF-1:hexasaccharide **1** complex, in comparison with free FGF, analyzed in terms of the reduced spectral density mapping as well as of the model-free approach, is described. As far as we know, this is the first study of this kind with sulfated-GAG activated FGFs. Previous similar studies have been performed using small molecules able to functionally emulate natural heparins (Chi et al., 2000), since the oligomerization of FGFs induced by natural heparin prohibits the sort of approaches used in the studies here reported. In combination with our previous and current studies on the structure of free and complexed FGF-1 (Pineda-Lucena et al., 1994, 1996 and results in preparation), the results presented here may represent a further step toward understanding the structural and dynamical basis of the recognition and activation of FGF-1 by HS-GAGs.

Materials and methods

Sample preparation

The FGF-1 gene was cloned between the NcoI and HindIII restriction sites in pRAT-4 (Peränen et al., 1996). Protein expression was carried out in *Escherichia coli* BL21(DE3). Uniformly labeled ^{15}N and ^{15}N, ^{13}C double-labelled FGF-1 polypeptides were obtained by growing the cells in M9 minimal media, using $^{15}NH_4Cl$ and ^{13}C glucose as the nitrogen and carbon sources, respectively. The protein was purified by affinity chromatography on a heparin-Sepharose column and was eluted at 1.5 M NaCl concentration.

For NMR studies, the buffer of the protein solution was changed by ultrafiltration to 10 mM sodium phosphate (pH 6.0) containing 150 mM NaCl and 1 mM hexasaccharide in the case of the complex samples, and 300 mM NaCl for the free protein. A higher NaCl concentration was used for free FGF-1, since the protein in the absence of heparin analogues is not stable below 300 mM NaCl. This concentration was not employed for the sugar-bound species to ensure the existence of the molecular complex. Previous experiments, using different NaCl concentrations showed that for the used concentrations in our NMR

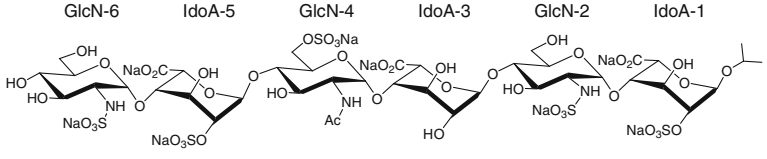

Figure 2. Structure of the heparin-like hexasaccharide analogue used in this study.

experiments, with a salt concentration of 150 mM, all the protein in solution is bound to the ligand. All samples were prepared in a mixture 90 % H_2O/ 10% ^2H_2O to give a final protein concentration of 1 mM in the NMR tube.

NMR experiments

NMR relaxation measurements were performed at 298 K on Varian Inova-750, and Bruker DRX-500 spectrometers with external magnetic field intensities of 17.6 and 11.7 T, respectively.

For assignment purposes, the three-dimensional NOESY-HSQC and TOCSY-HSQC were performed at 750 MHz with mixing times of 150 and 60 ms, respectively, using standard pulse sequences (Cavanagh et al., 1996). The numbers of acquired complex points were 2048 × 96 × 32 in the $t_3(^1H)$, $t_2(^1H)$ and $t_1(^{15}N)$, respectively. Thirty two scans (NOESY-HSQC) and 24 scans (TOCSY-HSQC) per increment were used. (3D) HNCA and (3D) HN(CO)CA were acquired at 800 MHz with 2048 × 64 × 64 complex points in the $t_3(^1H)$, $t_2(^{15}N)$ and $t_1(^{13}C)$, respectively. Thirty two scans (in HNCA) and 48 scans in HN(CO)CA were used. Spectral widths were 5600 Hz (^1H), 2800 Hz (^{15}N) and 6500 Hz (^{13}C).

^{15}N R_1, R_2 and steady-state heteronuclear $\{^1H\}$-^{15}N NOE experiments were carried out by using standard pulse sequences (Palmer, 1993; Farrow et al., 1994). Relaxation delays of 40, 60, 140, 240, 360, 520, 720, and 1200 ms (T_1 750 MHz); 10, 30, 50, 70, 90, 110, 130, and 150 ms (T_2 750 MHz); 40, 60, 140, 360, 520, 720, and 1200 ms (T_1 500 MHz); 20, 40, 60, 70, 90, 110, 130, and 150 ms (T_2 500 MHz) were employed. Recycle delays of 1.8 s for the T_1 experiments and 1.9 s for the T_2 measurements were used. Heteronuclear $\{^1H\}$–^{15}N NOE were determined from the ratio of two experiments with and without saturation. The saturation was carried out with a 3 s high power pulse train with a 5 s recycle delay. Sixteen scans in T_1, T_2 for the 750 MHz experiments were acquired, while 32 scans were used for 500 MHz. Forty eight scans were acquired for all $\{^1H\}$–^{15}N NOE experiments. All the experiments were obtained with 2048 × 256 complex points and the same spectral widths described above for the 3D experiments. The relaxation experiments were processed with the MestRe-C v3.0 software (Cobas and Sardina, 2003). T_1 and T_2 values were calculated by fitting the intensity of the peaks to a single exponential decay function.

Two methods were employed to characterize the dynamics of the free and bound states. Since R_1, R_2 and heteronuclear NOE values cannot be directly used to characterize the N–H dynamics, it is necessary to employ a method that relates the observed relaxation rates to the motional properties of the system. Indeed, the so-called *Model free approach* allows overcoming this difficulty, although it is necessary to assume a model to describe the motions of the system. The spectral density mapping approach also allows transfer the dynamic information contained in the relaxation parameters into motional properties of the system, but in this case no assumptions are required about a specific molecular model. Therefore, we feel that it is interesting to compare model-free with spectral density mapping-results, since the last methodology directly exploits the dynamic information contained in the relaxation rates without any *a priori* assumptions.

Reduced spectral density mapping

The spectral density mapping approach can be used to describe the existing intramolecular motions without using any assumptions about a specific molecular model. It is well-known that the heteronuclear relaxation parameters can be obtained from a weighted sum of the spectral density function, $J(\omega)$, sampled at specific frequencies. In a two-spin system such as ^{15}N–^1H, five frequencies are required: 0, ω_N, ω_H, ω_H–ω_N, $\omega_H + \omega_N$ (Peng and Wagner, 1992a, b). However, with the assumption that at high frequencies, the spectral density functions: $J(0.87\omega_H) \approx J(\omega_H + \omega_N) \approx J(\omega_H - \omega_N)$ (Farrow et al., 1995), it is possible to map the spectral density function using only three relaxation rates: R_1, R_2 and the ^1H–^{15}N cross relaxation rate constant, σ. Thus, the reduced spectral density values can be expressed as follows:

$$J(0) = [6R_2 - 3R_1 - 2.72\sigma]/[3d^2 + 4c^2] \quad (1)$$

$$J(\omega_N) = [4R_1 - 5.00\sigma]/[3d^2 + 4c^2] \quad (2)$$

$$J(0.87\omega_H) = 4\sigma/(5d^2) \quad (3)$$

where $d = \mu_0 h\gamma_N\gamma_H < r_{NH}^{-3} > /(8\pi^2)$, $c = \omega_N(\sigma_{||} - \sigma_\perp)/\sqrt{3}$, $\sigma = (\mathrm{NOE} - 1)R_1\gamma_N/\gamma_H$, μ_0 is the permeability of the free space, γ_H it and γ_N are the gyromagnetic ratios of ^{1}H and ^{15}N, respectively, h is Planck's constant; ω_N and ω_H are the Larmor frequencies of ^{1}H and ^{15}N, respectively, and r_{NH} is the N–H bond length. An axially symmetric chemical shift tensor has been assumed for ^{15}N with $\sigma_{||} - \sigma_\perp = -160$ ppm (Hiyama et al., 1988). The $J(0)$ values are affected by slow micro- to millisecond motions, the presence of this motions increasing the values.

Thus, the spectral density functions were mapped at five frequencies 0, 50, 500, 75, 750 MHz for the free protein and the complex. The $J(\omega)$ values and their uncertainties were calculated with the program anal_roe, kindly provided by Dr M. Guenneugues.

The spectral density mapping approach also provides information about the overall correlation time of the molecule, τ_m. The correlation time can be calculated from the Lefèvre equation (Lefèvre et al., 1996):

$$2\alpha\omega_N^2\tau_m^3 + 5\beta\omega_N^2\tau_m^2 + 2(\alpha - 1)\tau_m + 5\beta = 0 \quad (4)$$

The α and β coefficients are obtained by the linear least squares fit of $J(\omega_N)$ versus $J(0)$ values, $J(\omega_N) = \alpha\, J(0) + \beta$.

Model free analysis

The model free formalism (Lipari and Szabo, 1982) was also used to analyze the relaxation data. In this formalism, the spectral density function is modelled differently depending on whether the rotational diffusion tensor is either isotropic or anisotropic. In the isotropic movement, the spectral density function can be described as follows:

$$J(\omega) = \frac{2}{5}\left[\frac{S^2\tau_m}{1 + (\omega\tau_m)^2} + \frac{(1 - S^2)\tau}{1 + (\omega\tau)^2}\right] \quad (5)$$

where $\tau^{-1} = \tau_e^{-1} + \tau_m^{-1}$, S^2 is the generalised order parameter and specifies the degree of spatial restriction of the NH bond, τ_m is the correlation time for overall tumbling and τ_e is the correlation time for internal motion. It is also possible to take into account, an additional fast motion with a shorter correlation time, with the consequent expression resulting as:

$$J(\omega) = \frac{2}{5}S_f^2\left[\frac{S_s^2\tau_m}{1 + (\omega\tau_m)^2} + \frac{(1 - S_s^2)\tau}{1 + (\omega\tau)^2}\right] \quad (6)$$

where $\tau^{-1} = \tau_e^{-1} + \tau_m^{-1}$, S_s^2 and S_f^2 are the generalised order parameters for the relatively slow and fast motions, while $S^2 = S_s^2 S_f^2$, provided that these two motions are independent and axially symmetric.

The model-free analysis was performed by using the TENSOR2 program (Dosset et al., 2000). This program analyses the diffusion parameters of the system before studying the internal motions. TENSOR2 searches for the spectral density function that better reproduces the experimental data for each ^{1}H–^{15}N bond (Equations 7–9; Abraham, 1961). The program uses five models. Model 1 assumes that for fast internal movements, it is possible to reproduce the experimental relaxation parameters adjusting only one parameter (S^2). Since τ_e is very short, the second term of Equation 5 does not contribute to the spectral density function. Model 2 fits two parameters S^2 and τ_e. Model 3 is similar to Model 1 but takes into account the contribution of chemical exchange processes on the microsecond-millisecond to R_2 (R_{ex}, Equation 8). Model 4 is similar to Model 2 but including the R_{ex} term. Model 5 uses the spectral density function described in Equation 6 and fits three parameters S_s^2, S_f^2 and τ_e

$$R_1 = (d/2)^2[J(\omega_H - \omega_N) + 3J(\omega_N) + 6J(\omega_H + \omega_N)] + c^2J(\omega_N) \quad (7)$$

$$R_2 = 1/2(d/2)^2[4J(0) + J(\omega_H - \omega_N) + 3J(\omega_N) + 6J(\omega_H) + 6J(\omega_H + \omega_N)] + (1/6)c^2[4J(0) + 3J(\omega_N)] + R_{ex} \quad (8)$$

$$\mathrm{NOE} = 1 + (d/2)^2(\gamma_H/\gamma_N)[6J(\omega_H + \omega_N) - J(\omega_H - \omega_N)]/R_1 \quad (9)$$

Results

Chemical shift perturbation

The first step in the interaction study was a chemical shift perturbation analysis of the FGF-1 ^{1}H and ^{15}N NMR resonances upon addition of hexasaccharide **1**. Figure 3a shows the superimposition of the ^{1}H–^{15}N HSQC spectra for free and bound FGF-1. A relatively high number of NH groups are indeed affected by sugar binding. A plot of the chemical shift variations along the protein sequence is depicted in Figure 3b. The residues that show the largest changes are N32, H55, L87, H116, G124, G129, K132, G134, R136, H138, Y139, and I144. It can be observed that the

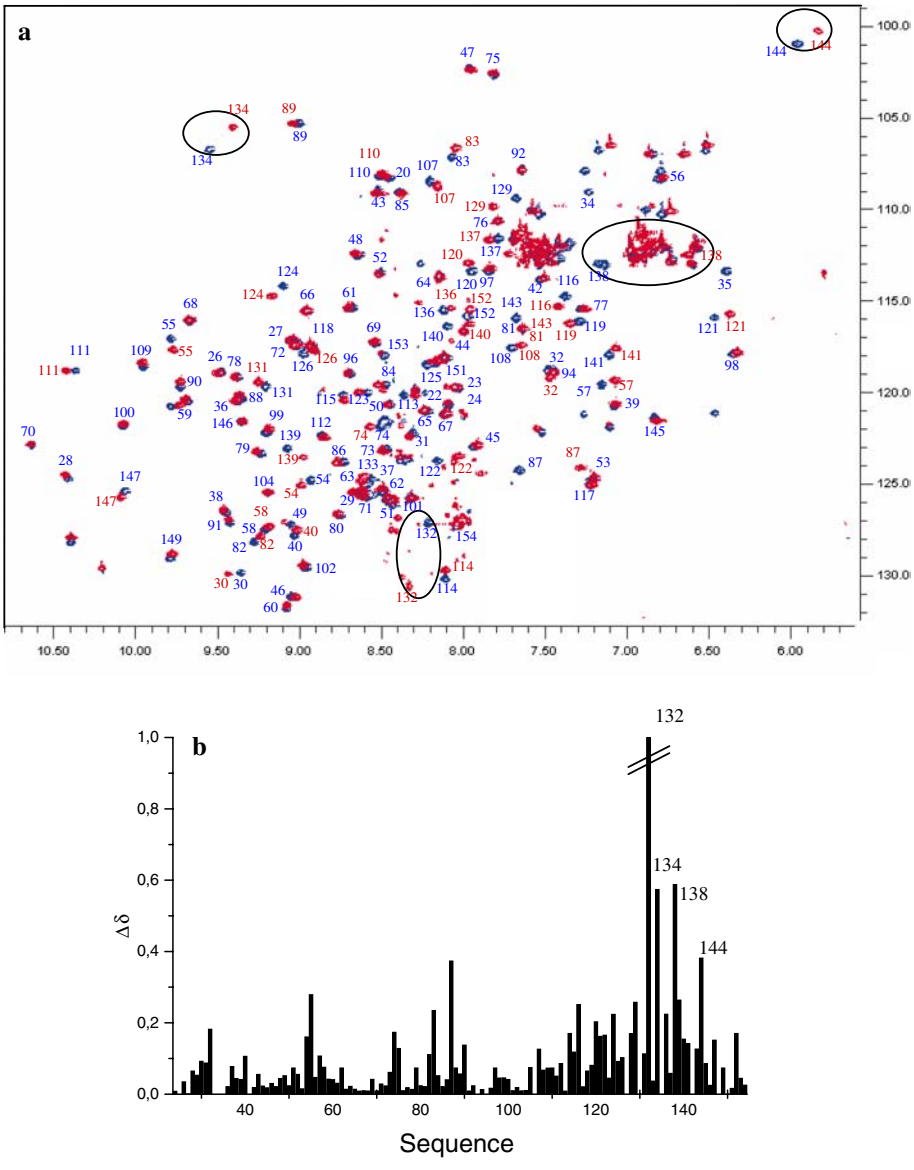

Figure 3. Chemical shift perturbation analysis. (a) Overlaid ^{1}H–^{15}N HSQC spectra of free (blue) and bound FGF-1 (red). The experiments were acquired at 17.6 T. (b) Weighted average (of ^{15}N and ^{1}H) chemical shift perturbation ($\Delta\delta = (\Delta\delta_H^2 + 0.2\Delta\delta_N^2)^{1/2}$) of FGF-1 residues upon complex formation. Residues K132, G134, H138 and I144 display the highest chemical shift variations between the free and bound states.

higher shifts are located at the C-terminus, especially at β-strands X and XI and at the loop connecting β-XI and β-XII. Interestingly, the observed perturbations are fairly similar for the interaction of FGF-1 with sucrose octasulfate (Chi et al., 2000) and are in agreement with the interacting residues found in the X-ray structures of FGF interacting with GAGs.

Field dependence of the ^{15}N R_1, ^{15}N R_2 and ^{1}H–^{15}N NOE

The relaxation parameters, R_1, R_2 and ^{1}H-^{15}N NOE were obtained from the analysis of proton detected ^{15}N and ^{1}H correlation spectra of the free FGF-1 and the FGF-1/hexasaccharide complex. Data were collected at 500 and 750 MHz for both forms. Backbone ^{1}H–^{15}N resonance assignments of the free and the hexasaccharide-complexed protein were determined using standard procedures (see Materials and methods). The R_1, R_2 and ^{1}H–^{15}N NOE data show the expected magnetic field dependence (Figure 4), with R_2 and ^{1}H–^{15}N NOE values increasing, and R_1 values decreasing with increasing magnetic field strength.

The mean relaxation parameters values are given in Table 1 to allow a comparative study between the free and the complexed form.

Averaged R_1, values for the free form are 1.61 s^{-1} at 11.7 T, that decrease at 1.48 s^{-1} upon complex formation. A reduction is also observed in this parameter when the measurements were taken at 17.6 T (from 0.84 to 0.80 s^{-1}). Our average R_2 values at both magnetic fields are very similar for both free and complexed forms, while they increase about 25% with the magnetic field from 11.7 to 17.6 T. The averaged NOE values also increase marginally 0.02 or 0.03 units upon binding at both magnetic fields, while they are about 0.1 units lower at 11.7 than at 17.6 T. The mean values for the free form are in good agreement with previously described results for human FGF-1, (Chi et al., 2000), especially for the averaged R_1 value, which was reported to be 1.61 s^{-1} at 11.7 T. The previously reported averaged R_2 and ^{1}H–^{15}N NOE steady state values at 500 MHz were 13.07 s^{-1} and 0.73, respectively, these values also are in fair agreement with our experimental observations, 13.69 s^{-1} and 0.69, respectively.

Regarding our data, the average R_1, R_2 and ^{1}H–^{15}N NOE values are similar for both free and hexasaccharide-bound forms. Nevertheless, it is possible to observe a systematic increase in the NOE values upon complex formation for most of the residues across the protein sequence, suggesting an overall increased ordering of the protein. The number of residues with high R_2 values decreases upon complex formation, which may indicate a change in the low frequency motions (μs to ms time scale). Both free and bound forms show relatively large R_1 values for some residues, which may indicate the presence of restricted mobility for these residues in the ps–ns time scale.

Reduced spectral density mapping approach

The measurement of R_1 and R_2 relaxation rates and ^{1}H–^{15}N NOE at 500 and 750 MHz for the free and complexed polypeptide allowed sampling of the spectral density function at a variety of frequencies, roughly 0, 50, 75, 500, and 750 MHz, corresponding to the $J(0)$, $J(\omega_N)$ and $J(\omega_H)$ values associated with the three fields. The obtained spectral density function values for the free and hexasaccharide-bound FGF-1 are plotted in Figure 5.

According to the obtained data, it is possible to observe that $J(0)$ is field dependent for several residues in both the free- and sugar-bound states. This fact seems to indicate that conformational exchange may indeed contribute to R_2, increasing the $J(0)$ value. In fact, under these conditions, $J(0)$ is expected to increase with the square of the magnetic field strength, assuming a two-site exchange and equal populations (Farrow et al., 1995).

It can be observed that the number of NH vectors with field dependence of $J(0)$ is much larger for free FGF-1 than for its hexasaccharide complex and are distributed along the protein sequence. These data globally indicate that chemical exchange within FGF-1 decreases upon sugar binding, and that the protein loses flexibility in the complex.

$J(\omega_N)$ and $J(\omega_H)$ values show the expected decreased with the increased of the magnetic field strength. $J(\omega_N)$ certainly shows uniform values along the protein sequence, this indicating that for the sampling frequencies, 50 and 75 MHz, the contribution of internal motions, faster than global motion, to the relaxation process is almost negligible. This effect is more noticeable at 75 MHz (Guignard et al., 2000).

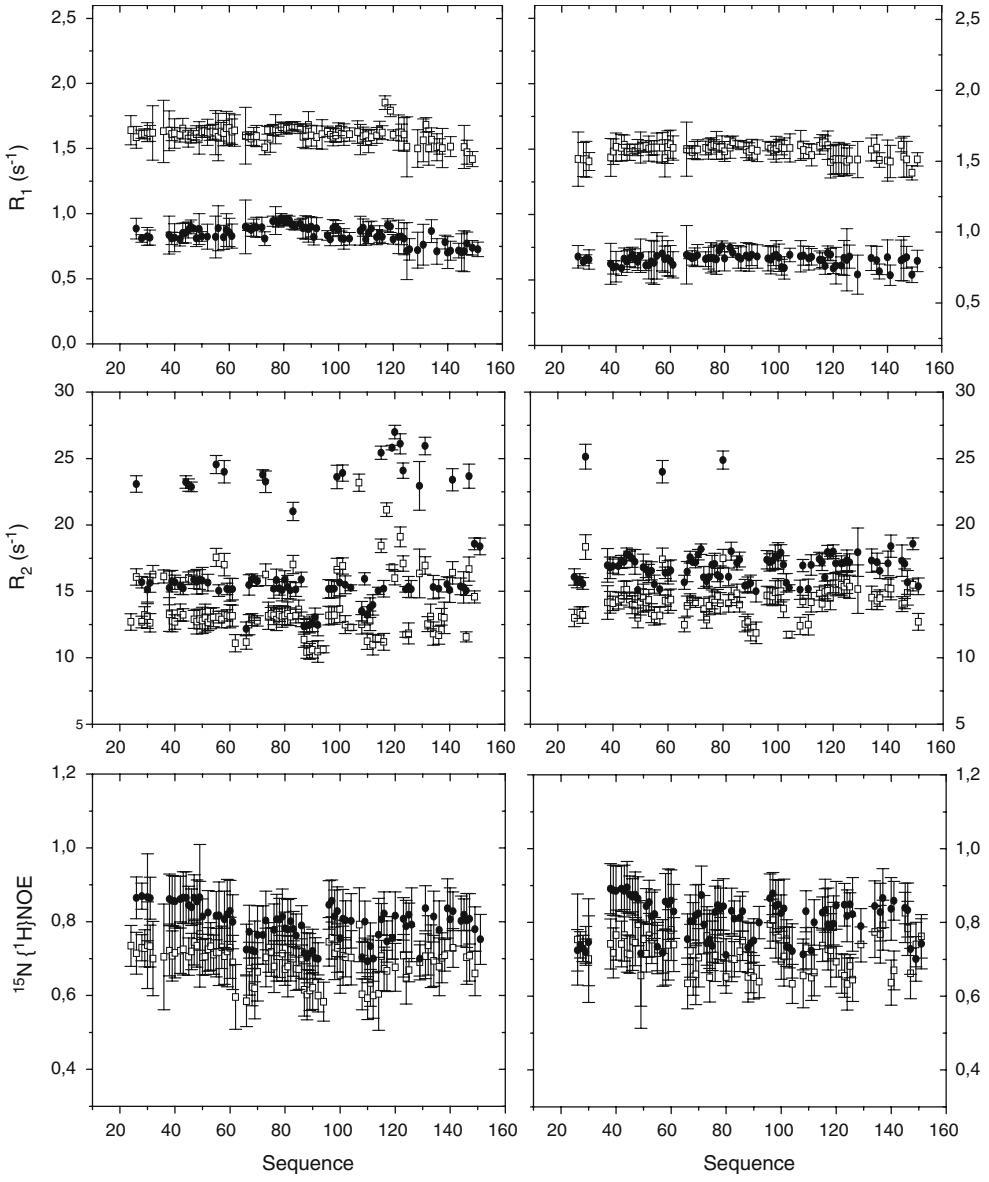

Figure 4. ^{15}N relaxation data R_1, R_2, and ^{15}N{^{1}H}NOE of uniformly ^{15}N labeled FGF-1, both in the free form (left panels) and in the FGF-1/hexasaccharide complex (right panels). Values at 11.7 and 17.6 T are represented as open squares and filled circles, respectively.

Table 1. Average values and standard deviations of the ^{15}N relaxation parameters for the free and hexasaccharide-complexed FGF-1

	Magnetic field (T)	< NOE >	$< R_1 >$ s^{-1}	$< R_2 >$ s^{-2}
Free	11.7	0.69 ± 0.07	1.61 ± 0.16	13.69 ± 0.66
Complex	11.7	0.72 ± 0.06	1.48 ± 0.16	14.30 ± 0.73
Free	17.6	0.79 ± 0.07	0.84 ± 0.15	17.37 ± 0.66
Complex	17.6	0.81 ± 0.07	0.80 ± 0.08	17.40 ± 0.65

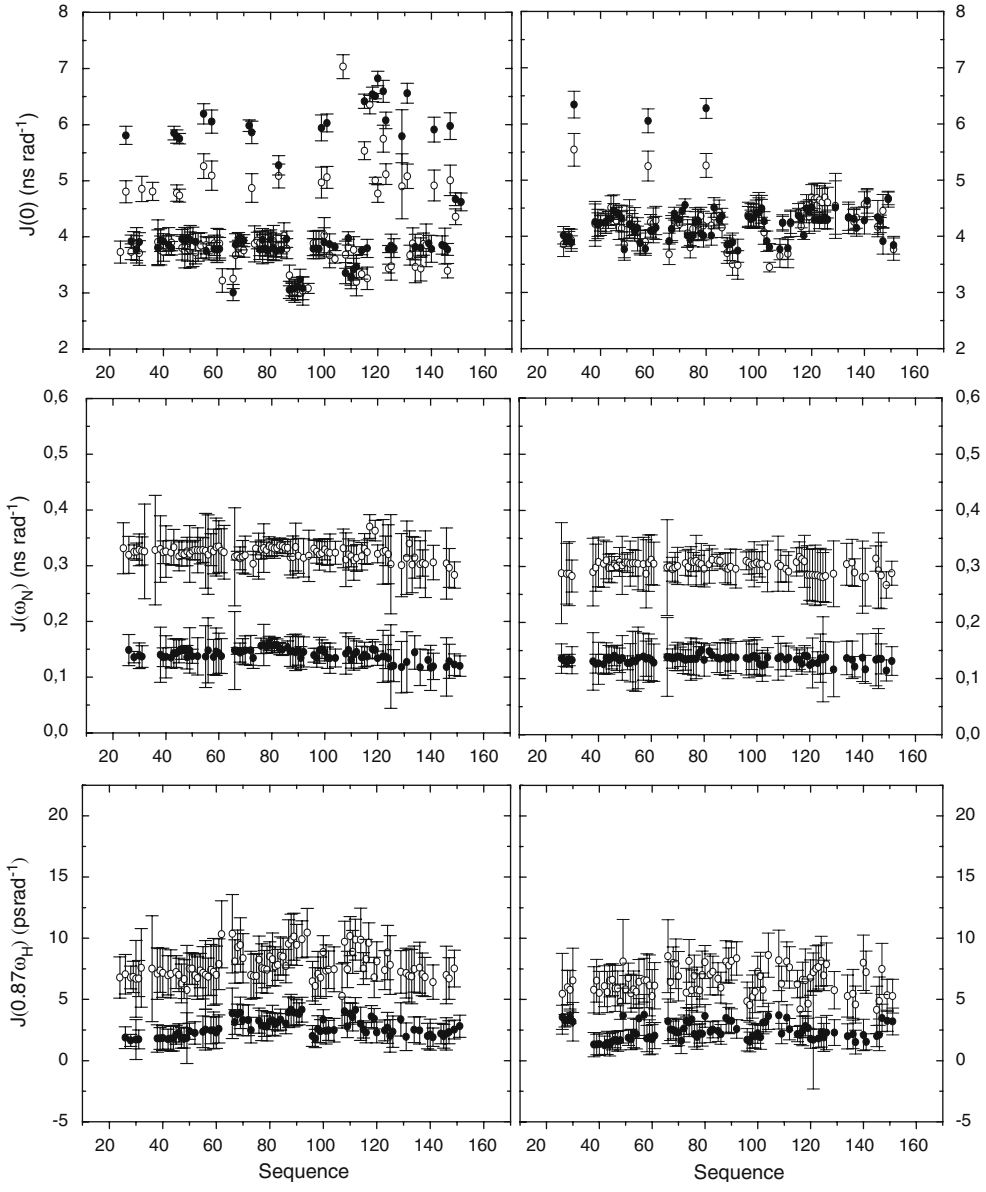

Figure 5. FGF-1 sequence distribution of the spectral density values mapped at the different frequencies. Open circles represent the data obtained at 11.7 T (0, 50 and 434 MHz) and filled circles represent the data at 17.6 T (0, 75 and 653 MHz). The left panels show the data for the free FGF-1 and right panels data for the FGF-1/hexasaccharide complex.

The binding of the hexasaccharide produces an overall decrease of the $J(\omega_N)$ and, very specially, of the $J(\omega_H)$ values, suggesting that globally the complex is much less dynamic in both the nano and picosecond timescales.

The overall correlation time, τ_m, can be determined from the linear correlation between $J(\omega_N)$ and $J(0)$, solving the Lefèvre equation as explained in Materials and Methods. The values obtained for τ_m from the 17.6 T data are 10.9 and 11.9 ns for the free and complex, respectively. These data are very much in agreement with the existence of a monomer for both the free and complexed forms.

Since, in the absence of chemical exchange and for similar nitrogen CSAs, the area under the spectral density curve, $J(\omega)$, is constant and should not vary for the different NH vectors (Slichter, 1990; Zhang et al., 1997), smaller $J(0)$ values

should be compensated by larger spectral density values at higher frequencies, approaching ω_N and/or ω_H. For instance, in the free protein, residues Gly 66 (at turn 3), Tyr 88, Gly 89 and Ser 90 (at β-VII), Thr 92 (loop 2) and Tyr 108, Tyr 111, and Ile 112 (β-strand IX) (all with low $J(0)$ values) have large $J(\omega_H)$ values. A similar trend takes place for the complexed form, for which residues Arg 49 (β-strand III), again Gly 66, Tyr 88, Gly 89 and Ser 90, Glu 104 (at β-strand VIII), and Tyr 108 (β-strand IX), (with low $J(0)$ values also) present the largest $J(\omega_H)$ values. These trends indicate that these residues experiment internal motions in the picosecond timescale.

Model free analysis

To provide additional insight into the backbone dynamics of the free and hexasaccharide-bound FGF-1, a Model Free analysis (Lipari and Szabo, 1982) of the experimental relaxation parameters at 11.7 and 17.6 T was also performed. For these magnetic fields, R_1, R_2 and ^1H–^{15}N NOE for both protein states were obtained. Model free analysis was performed with both datasets providing similar results, and therefore for the sake of simplicity, we only describe herein the model-free analysis (with TENSOR2) at the higher field. The 17.6 T experimental data (free and complex) were examined assuming either an isotropic or an anisotropic axially symmetric molecular tumbling model. The diffusion tensor components of the overall tumbling calculated by the program TENSOR2 (kindly provided by Dr P. Dosset) from the R_2/R_1 ratios were $D_{\|}/D_{\perp} = 0.94 \pm 0.2$ and $D_{\|}/D_{\perp} = 0.89 \pm 0.2$ for the free and complex, respectively. Since the model of anisotropic axially symmetric overall tumbling did not provide a statistically significant improvement in the fit and essentially gave the same results for the internal dynamics, it was concluded that the isotropic model adequately described the overall reorientation of the free and complex forms of the protein. The optimized isotropic correlation times, τ_m, were 10.4 ± 0.7 and 11.3 ± 0.6 ns for the free and FGF-1/hexasaccharide complex, respectively (similar to those obtained from the Lefèvre equation). The fit of the data allowed the description of a dynamic model for 83 spins (out of an input of 102) for the free, and for 84 spins for the complex form. For the free protein, 52 NH groups were adjusted to Model 1 (see Materials and Methods), 8 NH groups were adjusted to Model 2, while 22 and 1 were adjusted to Models 3 and 4, respectively. In contrast, for the complex, 75 NHs were adjusted by Model 1, while only 5, 2, and 2 NH groups were adjusted by models 2, 3, and 4, respectively (see Figure 6). The order parameters S^2 (which give information about motions occurring in the pico-nanosecond timescale), and the exchange broadening factors R_{ex} (which may arise from conformational exchange contributions occurring in a slower

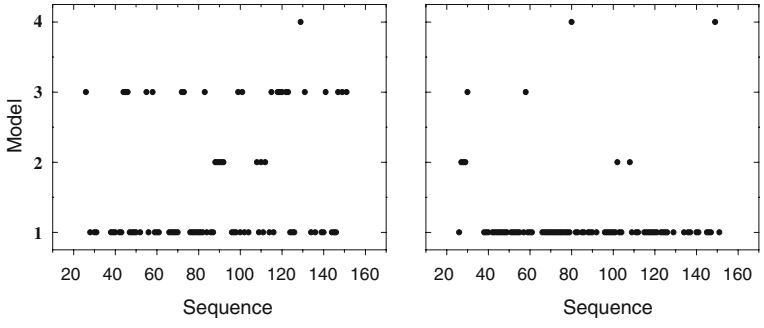

Figure 6. Schematic representation of the dynamic model that better reproduces the experimental data for each ^{15}N-^1H pair after the model-free analysis (model 1 (S^2); model 2 (S^2, τ_e); model 3 (S^2, R_{ex}); model 4 (S^2, τ_e, R_{ex})). Left panel: free FGF-1. Right panel: the FGF-1/hexasaccharide complex.

Figure 7. Model-free analysis. (a) Sequence distribution of order parameters (S^2) for free FGF-1 (top), for the FGF-1/hexasaccharide complex (middle) and $\Delta S^2 = S^2_{\text{free protein}} - S^2_{\text{complex}}$ (bottom). The horizontal dotted lines (top and middle panels) represent the mean values for S^2. (b) Chemical exchange contributions to R_2 relaxation rates for free FGF-1 (left) and for the FGF-1/hexasaccharide complex (right).

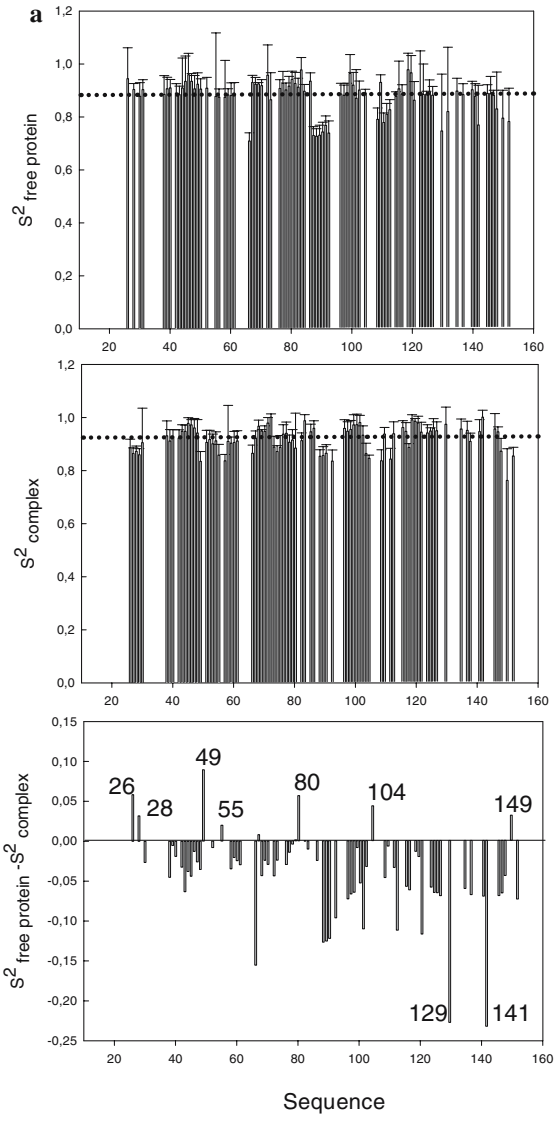
a
S2 free protein
S2 complex
S2 free protein -S2 complex
26
28
49
55
80
104
129
141
149
Sequence

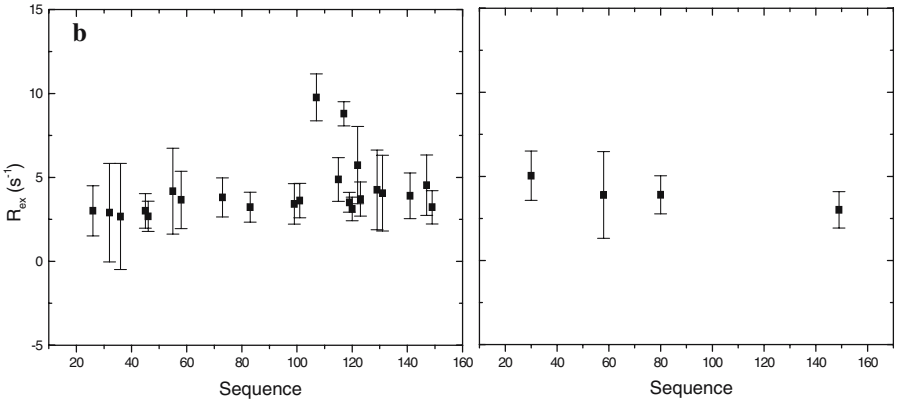
b
Rex (s-1)
Sequence
Sequence

timescale around micro to milliseconds), are plotted in Figures 7a–b.

The average S^2 value for the free and the complex do not vary significantly and indeed are within the error range, 0.87 ± 0.06 and 0.92 ± 0.04, respectively. There are not significant differences among the different protein regions. Indeed, residues exhibiting more restricted dynamics ($S^2 > 0.9$) and those experimenting rapid motions ($S^2 < 0.8$) are distributed throughout the protein sequence, including the β-strands and the loops, for both the free and complexed forms. For both free and bound FGF-1, the NH groups with smaller S^2 values correspond with those that show low $J(0)$ and high $J(\omega_H)$ values. Thus, residues Gly 66 (turn 3), Tyr 88, Gly 89 and Ser 90 (β-strand VII), y Tyr 108 (β-strand IX) show fast motions in the picoseconds timescale in both protein forms. In addition, Thr 92 (loop 2), Tyr 111 and Ile 112 (β-strand IX) of free FGF-1 and Arg 49 (β-strand III) and Glu 104 (β-strand VIII) of the complexed form are also affected by motions within this timescale.

The differences in order parameter between the free and bound FGF-1 (see Figure 7a, bottom) show that most of the residues lose flexibility upon binding. The most affected NH groups correspond to the C-terminus, several of them, as Leu 125 ($\Delta S^2 = 0.06$), Lys 126 ($\Delta S^2 = 0.07$), Gly 129 ($\Delta S^2 = 0.23$), Gly 134 ($\Delta S^2 = 0.06$), Arg 136 ($\Delta S^2 = 0.07$) and Gln 141 ($\Delta S^2 = 0.23$) are close to the hexasaccharide binding site. Indeed, the NH moieties of these aminoacid residues show significant chemical shift perturbations upon binding: Leu 125, $\Delta\delta = 0.09$ ppm; Lys 126, $\Delta\delta = 0.10$ ppm; Gly 129 $\Delta\delta = 0.26$ ppm; Gly 134 $\Delta\delta = 0.57$ ppm; Arg 136 $\Delta\delta = 0.22$ ppm; Gln 141 $\Delta\delta = 0.14$ ppm (see Figure 3).

However, not all the residues do rigidify upon hexasaccharide binding. Residues Lys 26 and Leu 28 (β-strand I), Arg 49 (β-strand III), His 55 (loop 1), Ala 80 (β-strand VI), Glu 104 (β-strand VIII) and Leu 149 (β-strand XII) show a smaller order parameter value in the bound form (Figure 7a).

A difference is observed between both forms regarding the contribution of chemical exchange (see Figures 6 and 7b). In the micro to millisecond timescale, 23 residues of the free FGF-1 required the exchange factor, R_{ex}, for a proper fit of the data, while only 4 were required for the FGF-1/hexasaccharide complex (see also Figures 6 and 7b). Residues experimenting contribution from exchange in the free form are Lys 26 (β-strand I), Thr 44, Val 45 and Asp 46 (β-strand III), His 55 (loop 1), Leu 58 (β-strand IV), Ser 72 (β-strand V), Thr 73 (turn 4), Thr 83 (turn 5), Phe 99 and Glu 101 (β-strand VIII), Lys 115, Glu 118, Lys 119, Asn 120, Phe 122 (loop 3), Val 123 (β-strand X), Gly 129 (turn 7), Cys 131 (β-strand XI), Gln 141 (loop 4), Leu 147 and Leu 149 (β-strand XII), Val 151 (end terminal region). The only residues with contribution from exchange in the complex form are Cys 30 (β-strand I), Leu 58 (β-strand IV), Ala 80 (β-strand VI) and Leu 149 (β-strand XII). These results permit to confirm that the chemical exchange process are less important upon sugar complexation.

Discussion

Fast dynamics in the ps to ns timescale

Interestingly, the monomeric complex found in this biologically active FGF1 bound to the heparin-like hexasaccharide has permitted to access to detailed dynamic information, that has not been available for the dimeric forms obtained when oligosaccharides of the regular region of heparin are used.

The Model Free analysis has indicated that the acidic Fibroblast Growth Factor (FGF-1) is rather flexible in the fast pico-nanosecond dynamic timescales. Interestingly, a good correlation has been found with residues that experiment less protection against amide proton exchange (Chi et al. 2002) and with residues exhibiting lower S^2 (higher flexibility) and higher $J(\omega_H)$ values in the free protein. Herein, the average value of the order parameter S^2 of the amide N-H pairs is only slightly higher after binding to the hexasaccharide, with interesting differences when the comparison is performed at the residue level (Figure 7a). For several residues across the whole sequence, but very specially for those located in the last β strands, IX to XII, S^2 significantly increased when bound to the hexasaccharide. Interestingly, this is also the region that exhibits the highest chemical shift changes between the free and hexasaccharide-bound states (Figure 3a–b) that most likely corresponds to the HS-GAG binding site (results in preparation). Besides these residues,

and as described above, there are other (much fewer) amide pairs that show smaller S^2values (Figure 7a).

In several instances, minor discrepancies between FGF solution and crystal structures have been reported, especially on the existence or not of β-strand XI in solution. Our analysis indicate that the order parameter substantially increase (0.19 units) in this region. Thus, the flexibility for these residues could preclude the observation of intramolecular nuclear Overhauser effects characterizing β-strand XI. Our NMR chemical shift perturbation analysis together with intermolecular NOE data (in preparation) has shown that residues in β-strand XI are indeed involved in heparin binding in solution. Thus, it seems that the existing flexibility of the residues at β-strand XI in the free state could possibly favor complex formation with the heparin oligosaccharides by lowering the free energy barrier.

Similarly, higher flexibility in the bound form of Arg 49, Leu 149, and Tyr 108 residues also might be indeed biologically relevant, since it has been described that Arg 49 and Leu 149, together with Tyr 108 (which is rather flexible for both free and bound states) provide interaction spots for the FGF receptor (Springer et al., 1994; Pellegrini et al., 2000). Thus, the observed flexibility for these residues in the hexasaccharide-bound state might be associated to the capacity of FGF-1 to interact with seven of the presently known FGFRs (Ornitz et al., 1996).

The molecular basis for protein target binding is controlled by a variety of factors including favorable binding enthalpy, changes in solvent, side chain, and backbone entropies of the interaction partners (Forman-Kay, 1999; Cavanagh and Akke, 2000). The conformational entropy contribution to the free energy of binding can be estimated from the order parameters as described by Akke (Akke et al., 1993a).

$$\Delta G = G_{\text{complex}} - G_{\text{free}} = -RT\,\Sigma \ln[1 - S^2_{\text{complex}})/(1 - S^2_{\text{free}})] \quad (10)$$

where R is the molar gas constant, S^2 is the order parameter and G is the free energy of Gibbs.

In the FGF-1 case, according to the order parameters variation, complex formation leads to an unfavorable entropic contribution to the free energy of binding at 298 K of $\approx$ 22 kcal/mol. Although some cases of increase in flexibility upon binding have been recently reported, which might be attributed to compensate for the release of structured water (Morton and Matthews, 1995; Stone et al. 2001; Favier et al. 2002; Fayos et al. 2003), most of the NMR relaxation studies carried out for molecular complexes have permitted to deduce a decrease in the fast internal motions upon binding. This is also is the case for FGF-1 upon binding to the heparin-related hexasaccharide **1**. Thus, sugar binding is associated with a loss of conformational entropy, which is necessarily offset by increases in solvent entropy and/or the formation of favorable enthalpic interactions. (Krishnan et al., 2000; Dyson and Wright, 2001; Osborne et al., 2001). Due to the similarities found in the structure and the backbone dynamics of the protein interleukin 1β and FGF-1, some authors have suggested (Chi et al. 2000) that the high flexibility observed in the binding regions of the free forms could be the basis for cytokine activity exhibited by these proteins.

Slow dynamics in the μs to ms range

For the free form, the residues that experiment contribution from chemical exchange are not distributed in a concrete region of the protein backbone, but are spread throughout the complete sequence.

After binding to the hexasaccharide, the contribution from exchange decreases globally. As suggested by several authors (Nicholson et al., 1992; Akke et al., 1993b; Farrow et al., 1994; Epstein et al., 1995; Stivers et al., 1996), conformational exchange may be a mechanism to control the lost (or gain) of the entropy of binding, modulating the available intrinsic binding energy to preserve or favor the binding of the protein to specific targets. Indeed, the affinity of binding found for the FGF-1 to heparin binding is in the nanomolar range (Pineda-Lucena et al., 1996).

A variety of structural studies have been previously performed for different forms of free FGF-1 and bound to different simple ligands, which do not have the heparin structure. Additionally, a relaxation study has also been performed for FGF-1 bound to a simple disaccharide, sucrose octasulfate, also structurally far from the heparin family.

(Zhu et al., 1993; Pineda-Lucena et al., 1994; DiGabriele et al., 1998; Ogura et al., 1999; Chi et al., 2000, 2002). Although the exact role of these ligands in the activation of the FGF-1 signaling pathway is still not clear (Arunkumar et al., 2002b), it appears that ligand binding is a requirement for the protein activation and receptor binding.

The synthetic hexasaccharide studied here has shown to activate the FGF-1 monomer (Angulo et al., 2004) suggesting, consequently, that conformational exchange may be involved in controlling the activation, target recognition and biological function of the FGF-1, and that dimerization of FGF-1 does not show to be a prerequisite for activation.

Conclusions

Chemical shift perturbation analysis and backbone NMR relaxation studies on FGF-1, both in the free state and when bound to a heparin-based hexasaccharide have been performed. The analysis of the data has allowed us to extract information about the dynamics at different timescales (from picoseconds to milliseconds), using the Model Free formalism and spectral density mapping. The data unambiguously indicate that FGF does not dimerize in the presence of this designed synthetically prepared heparin-like hexasaccharide, in contrast with the results described for regular heparin hexasaccharides. Nevertheless, the complex is biologically active. The dynamic information obtained from the different analysis seems to be fairly consistent with each other. The main conclusion is that FGF-1 presents a variety of internal motions and chemical exchange in the free state, particularly at the heparin binding site, and that these motions decrease upon hexasaccharide binding, specially at the binding site region, in both the fast (pico-nanoseconds) and slow (micro-milliseconds) dynamic timescales. These observations suggest that the motions may be involved in the regulation of heparin binding and subsequent activation of FGF-1. The binding process is penalized with ca. 22 kcal/mol conformational entropy loss.

Acknowledgements

We thank Mrs. Mercedes Zazo for her help during the expression and purification of labelled FGF-1. This work was supported by the Dirección General de Investigación Científica y Técnica (Grants BQU2000-1501-C02-01, BQU2002-0374, and BQU2003-03550-C03-01). We are indebted to Dr Dosset and Dr Guenneugues for kindly providing the programmes TENSOR2 and anal_roe, respectively. We also thank Comunidad de Madrid, Fundación Ramón Areces, and Fundación Francisco Cobos for fellowships to R.F., J.A., and R.O., respectively. NMR time from the Parc Cientific of Barcelona (Dr. M. Gairí), University of Santiago de Compostela, and CAI-NMR of Universidad Complutense is warmly thanked.

References

Abraham, A. (1961) *The Principles of Nuclear Magnetism* Clarendon Press, Oxford.

Akke, M., Brüschweiler, R. and Palmer III, A.G. (1993a) *J. Am. Chem. Soc.*, **115**, 9832–9833.

Akke, M., Skelton, N.J., Kordel, J., Palmer III, A.G. and Chazin, W.J. (1993b) *Biochemistry*, **32**, 9832–9844.

Atwell, S., Ultsch, M., De Vos, A.M. and Wells, J.A. (1997) *Science*, **278**, 1125–1128.

Angulo, J., Ojeda, R., de Paz, J.L., Lucas, R., Nieto, P.M., Lozano, R.M., Redondo-Horcajo, M., Giménez-Gallego, G. and Martín-Lomas, M. (2004) *Chem. Bio. Chem.*, **5**, 55–61.

Arunkumar, A.I., Srisailam, S., Krishnaswamy, T., Kumar, S., Kathir, K.M., Chi, Y.-H., Wang, H.-M., Chang, G.-G., Chiu, I.-M. and Yu, C. (2002a) *J. Biol. Chem.*, **277**, 46424–46432.

Arunkumar, A.I., Kumar, T.K., Kathir, K.M., Srisailam, S., Wang, H.-M., Leena, P.S., Chi, Y.H., Chen, H.C., Wu, C.H., Wu, R.T., Chang, G.G., Chiu, I.M. and Yu, C. (2002b) *Protein Sci.*, **11**, 1050–61.

Capila, I. and Lindhardt, R.J. (2002) *Angew. Chem.*, **114**, 428–451.

Cavanagh, J., Fairbrother, W.J., Palmer III, A.G. and Skelton, N.J (1996) *Protein NMR Spectroscopy: Principles and Practice* Academic Press, San Diego, CA.

Cavanagh, J. and Akke, M. (2000) *Nat. Struct. Biol.*, **7**, 11–3.

Chi, Y., Kumar, K.S., Chiu, I.-M. and Yu, C. (2000) *J. Biol. Chem.*, **275**, 39444–50.

Chi, Y.-H., Kumar, T., Kathir, K., Lin, D.-H., Zhu, G., Chiu, I.-M. and Yu, C. (2002) *Biochemistry*, **41**, 15350–15359.

Clackson, T. and Wells, J.A. (1995) *Science*, **267**, 383–386.

Cobas, J.C. and Sardina, F.J. (2003) *Concepts Magn. Reson.*, **19A**, 80–96.

Conrad, H.E. (1998) *Heparin-Binding Proteins* Academic Press, San Diego.

DiGabriele, A.D., Lax, I., Chen, D.I., Svahn, C.M., Jaye, M., Schlessinger, J. and Hendrickson, W.A. (1998) *Nature*, **393**, 812–817.

Dosset, P., Hus, J.C., Blackledge, M. and Marion, D. (2000) *J. Biomol. NMR*, **16**, 23–28.

Dyson, H.J. and Wright, P.E. (2001) *Methods Enzymol.*, **339**, 258–70.

Epstein, D.M., Benkovic, S.J. and Wright, P.E. (1995) *Biochemistry*, **34**, 11037–48.
Faham, S., Hileman, R.E., Fromm, J.R., Lindhardt, R.J. and Rees, D.C. (1996) *Science*, **271**, 1116–1120.
Faham, S., Lindhardt, R.J. and Rees, D.C. (1998) *Curr. Opin Struct. Biol.*, **8**, 578–586.
Farrow, N.A., Muhandiram, R., Singer, A.U., Pascal, S.M., Kay, C.M., Gish, G., Shoelson, S.E., Pawson, T., Forman-Kay, J.D. and Kay, L.E. (1994) *Biochemistry*, **33**, 5984–6003.
Farrow, N.A., Zhang, O., Szabo, A., Torchia, D.A. and Kay, L.E. (1995) *J. Biomol. NMR*, **6**, 153–62.
Favier, A., Brutscher, B., Blackledge, M., Galinier, A., Deutscher, J., Penin, F. and Marion, D. (2002) *J. Mol. Biol.*, **317**, 131–44.
Fayos, R., Melacini, G., Newlon, M.G., Burns, L., Scott, J.D and Jennings, P.A. (2003) *J. Biol. Chem.*, **278**, 18581–7.
Feher, V.A. and Cavanagh, J. (1999) *Nature*, **400**, 221–222.
Forman-Kay, J.D. (1999) *Nat. Struct. Biol.*, **6**, 1086–1087.
Giménez-Gallego, G., Rodkey, J., Bennett, C., Rios-Candelore, M., DiSalvo, J. and Thomas, K. (1985) *Science*, **230**, 1385–1388.
Giménez-Gallego, G. and Cuevas, P. (1994) *Neurolog. Res.*, **16**, 313–316.
Guignard, L., Padilla, A., Mispelter, J., Yang, Y.S., Stern, M.H., Lhoste, J.M. and Roumestand, C. (2000) *J. Biomol. NMR*, **17**, 215–230.
Harmer, N.J., Pellegrini, L., Chirgadze, D., Fernández Recio, J. and Blundell, T.L. (2004a) *Biochemistry*, **43**, 629–640.
Harmer, N.J., Ilag, L.L., Mulloy, B., Pellegrini, L., Robinson, C.V. and Blundell, T.L. (2004b) *J. Mol. Biol.*, **339**, 821–834.
Hiyama, Y., Niu, C.-H., Silverton, J.V., Bavoso, A. and Torchia, D.A. (1988) *J. Am. Chem. Soc.*, **110**, 2378–2383.
Itoh, N. and Ornitz, D.M. (2004) *Trend. Gen.*, **20**, 563–569.
Korzhnev, D.M., Billeter, M., Arseniev, A.S. and Orekhov, V.Y. (2001) *Prog. Nucl. Magn. Reson. Spectrosc.*, **38**, 197–266.
Krishnan, V.V., Sukumar, M., Gierasch, L.M. and Cosman, M (2000) *Biochemistry*, **39**, 9119–9129.
Lefèvre, J.-F., Dayie, K.T., Peng, J.W. and Wagner, G. (1996) *Biochemistry*, **35**, 2674–2686.
Lipari, G. and Szabo, A. (1982) *J. Am. Chem. Soc.*, **104**, 4546–4570.
McLachlan, A.D. (1979) *J. Mol. Biol.*, **133**, 557–563.
Mohammadi, M., Olsen, S.K. and Goetez, R. (2005a) *Curr. Opin. Struct. Biol.*, **15**, 506–516.
Mohammadi, M., Olsen, S.K. and Ibrahimi, O.A. (2005b) *Cytok. Growth. Fact. Rev.*, **16**, 107–137.
Morton, A. and Matthews, B.W. (1995) *Biochemistry*, **34**, 8576–8588.
Moy, F., Seddon, A., Campell, E., Bohlen, P. and Powers, R. (1995) *J. Biomol. NMR*, **6**, 245–254.
Nicholson, L.K., Kay, L.E., Baldisseri, D.M., Arango, J., Young, P.E., Bax, A. and Torchia, D.A. (1992) *Biochemistry*, **31**, 5253–63.
Nishimura, T., Nakatake, Y., Konishi, M. and Itoh, N. (2000) *Biochim. Biophys. Acta*, **1492**, 203–206.
Ogura, K., Nagata, K., Hatanaka, H., Habuchi, H., Kimata, K., Tate, S.-I., Ravera, M., Jaye, M., Schlessinger, J. and Inagaki, K. (1999) *J. Biomol. NMR*, **13**, 11–24.
Ornitz, D., Yayon, A., Flanagan, J., Svahn, C., Levi, E. and Leder, P. (1992) *Mol. Cell. Biol.*, **12**, 240–247.
Ornitz, D.M., Xu, J., Colvin, J.S., Mc Ewen, D.G., Mac Arthur, C.A., Coulier, F., Gao, G. and Goldfarb, M. (1996) *J. Biol. Chem.*, **271**, 15292–15297.
Osborne, M.J., Schnell, J., Benkovic, S.J., Dyson, H.J. and Wright, P.E. (2001) *Biochemistry*, **40**, 9846–59.
Palmer, A.G. (1993) *Curr. Opin. Biotechnol.*, **4**, 385–391.
Pellegrini, L., Burke, D.F., von Delft, F., Mulloy, B. and Blundell, T.L. (2000) *Nature*, **407**, 1029–1034.
Pellegrini, L. (2001) *Curr. Opin. Struct. Biol.*, **11**, 629–634.
Peng, J.W. and Wagner, G. (1992a) *J. Magn. Reson.*, **98**, 308–332.
Peng, J.W. and Wagner, G. (1992b) *Biochemistry*, **31**, 8571–8586.
Peränen, J., Rikkonen, M., Hyvönen, M. and Kääriänien, L. (1996) *Anal. Biochem.*, **236**, 371–373.
Pineda-Lucena, A., Jiménez, M.A., Nieto, J.L., Santoro, J., Rico, M. and Giménez-Gallego, G. (1994) *J. Mol. Biol.*, **242**, 81–98.
Pineda-Lucena, A., Jiménez, M.A., Lozano, R.M., Nieto, J.L., Santoro, J., Rico, M. and Giménez-Gallego, G. (1996) *J. Mol. Biol.*, **264**, 162–78.
Powers, C.J., Mc Leskey, S.W. and Wellstein, A. (2000) *Endocr. Relat. Cancer*, **7**, 65–97.
Rapraeger, A., Krufka, A. and Olwin, B. (1991) *Science*, **252**, 1705–1708.
Schlessinger, J., Plotnikov, A.N., Ibrahimi, O.A., Eliseenkova, O.A., Yeh, B.K., Yayon, A., Lindhardt, R.J. and Mohammadi, M. (2000) *Mol. Cell.*, **6**, 743–750.
Slichter, C. (1990) *Principles of Magnetic Resonance* Springer Verlag, New York.
Spivak-Kroizman, T., Lemmon, M.A., Dikic, I., Ladbury, J.E., Pinchsi, D., Huang, J., Jaye, M., Crumley, G., Schlessinger, J. and Lax, I. (1994) *Cell*, **79**, 1015–1024.
Springer, B.A., Pantoliano, M.W., Barbera, F.A., Gunyuzla, P.L., Thompson, L.D., Herblin, W.F., Rosendeld, S.A. and Book, G.W. (1994) *J. Biol. Chem.*, **269**, 26879–26884.
Stauber, D.J., Digabriele, A.D. and Hendrickson, W.A. (2000) *Proc. Natl. Acad. Sci. USA*, **97**, 49–54.
Stivers, J.T., Abeygunawardana, C. and Mildvan, A.S. (1996) *Biochemistry*, **35**, 16036–16047.
Stone, M.J., Gupta, S. and Snyder, N. (2001) *J. Am. Chem. Soc.*, **123**, 185–186.
Venkataraman, G., Shriver, Z., Davis, J.C. and Sasisekharan, R. (1999) *Proc. Natl. Acad. Sci. USA*, **96**, 1892–1897.
Waksman, G. and Herr, A.B. (1998) *Nat. Struct. Biol.*, **5**, 527–530.
White, K.E., Evans, W.E., O'Riordan, J.L., Speer, M.C., Econs, M.J., Lorenz-Depiereux, B., Grabowski, M., Meitinger, T. and Strom, T.M. (2000) *Nat. Genet.*, **26**, 345–348.
Wu, Z.L., Zhang, L., Yabe, T., Kuberan, B., Beeler, D.L., Love, A. and Rosenberg, R.D. (2003) *J. Biol. Chem.*, **278**, 17121–17129.
Yayon, A., Klagsbrun, M., Esko, J.D., Leder, P. and Ornitz, D.M (1991) *Cell*, **64**, 841–848.
Zhang, P., Dayie, K.T. and Wagner, G. (1997) *J. Mol. Biol.*, **272**, 443–55.
Zhu, X., Hsu, B.T and Rees, D.C (1993) *Structure*, **1**, 27–34.